B. E. Launder
Department of Mechanical Engineering,
University of California,
Davis, Calif. 95616

M. Leschziner
Sonderforschungsbereich, 80
University of Karlsruhe,
Karlsruhe, West Germany

Flow in Finite-Width, Thrust Bearings Including Inertial Effects

I—Laminar Flow

Presented is a new numerical procedure for the calculation of flow in finite-width bearing films. The method, based on the integro-differential approach, is a development of schemes devised by Patankar and Spalding [8] and Gosman and Pun [9] for general flows occurring in fields other than tribology. Principal features of the method are: the full inclusion of inertial effects; the retention of "primitive" variables; the use of a marching solution procedure using line-by-line solution of the discretized conservation equations. Applications to several aspects of laminar inertial flow problems are discussed.

1 Introduction

Within the extensive subject of hydrodynamic lubrication, the contribution of inertial influences to bearing performance has received relatively little attention. Analyses of lubricant flows have normally been based on the so-called Reynolds equation obtained from integrated forms of the momentum and continuity equations with all fluid-acceleration terms omitted. Kahlert [1] was perhaps the first to deduce that the importance of inertial terms depend upon the magnitude of the effective film Reynolds number, Re* defined as:

$$\mathrm{Re}^* \equiv \frac{Uh}{\nu}\frac{h}{L}$$

where U is the slider velocity, h and L are respectively, a typical film thickness and length of the bearing and ν is the kinematic viscosity. Kahlert [1], Brand [2] and others have shown that for laminar flow inertial effects became significant when the Reynolds number, defined as above, if of order unity. In many bearing applications effective film Reynolds numbers are so low as to justify entirely the neglect of acceleration terms. Nevertheless, with the trend towards increasing bearing loads, there is a growing number of applications where Re* exceeds unity.

The inclusion of inertial terms in the equations of motion very much complicates the task of solution. The pressure field can then no longer be decoupled from the field, and, moreover, the inertial terms are strictly non-linear. Some workers including Kahlert [1] and Kamal [3] have simplified the inertial terms in order to preserve the linearity of the equation set; by this means analytical methods of solution may be developed. The accuracy of such linearisations is rather hard to judge *a priori* however. Launder and Ying [4], for example, who obtained complete numerical solutions to the journal-bearing problem studied by Kamal, found their results were much closer to the non-inertial result than to the linearized inertial treatment of [3]. Thus, the only certain approach to including the acceleration terms is to retain the nonlinear terms in full—a practice which dictates that numerical solution procedures be employed.

The static pressure couples the momentum equations in a rather awkward way; moreover it does not appear as the dominant variable in either of the momentum equations or the continuity equation. For this reason many of the earlier numerical approaches have employed, for two-dimensional flows, the stream function and vorticity in place of the two momentum equations and the continuity equation. The well-documented procedure of Gosman, Pun, Runchal, Spalding, and Wolfshtein [5] is perhaps the most extensively used method of this kind. This approach has a disadvantage for lubrication problems: namely, that since the pressure distribution is the physical quantity of prime importance it needs to be recovered from the calculated values of stream function and vorticity. While this can be done—and has been [4]—the necessity to do so diminishes the attractiveness of this approach. This shortcoming has been avoided by Smalley, Vohr, Castelli, and Wachman [6] who employed the stream function and static pressure as dependent variables. This novel approach while interesting, is out of step with most other recent work on the development of solving schemes for the Navier Stokes equations. There is a growing emphasis on the retention of so-called "primitive" variables, i.e. the velocity components in orthogonal directions and the static pressure. General solution schemes of this kind have been reported by Patankar [7] and Patankar and Spalding [8] while Gosman and Pun [9] have provided a general FORTRAN coding of these schemes in the computer program TEACH. Our own work has taken these approaches as its starting point.

The present paper is the first of two documenting the development and application of a general numerical procedure for flow in finite width thrust bearings. The basic solving procedure and its application to establishing inertial influences in laminar flow are presented in succeeding sections; a companion paper [10] provides a new set of

Contributed by the Lubrication Division for publication in the JOURNAL OF LUBRICATION TECHNOLOGY. Manuscript received at ASME Headquarters, May 1, 1978.

 Copyright © 1978 by ASME

Downloaded 16 Aug 2012 to 165.91.101.108. Redistribution subject to ASME license or copyright; see http://www.asme.org/terms/Terms_Use.cfm

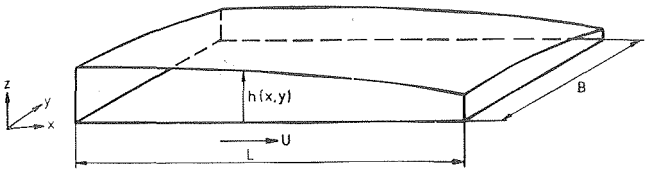

Fig. 1 Geometrical configuration

turbulent flow resistance laws which is believed to be more generally valid than earlier proposals with corresponding predictions of inertial effects.

2 Mathematical Formulation

We are concerned with the flow between two impermeable and rigid surfaces as indicated in Fig. 1; the lower surface moves with velocity U in the x direction and the upper surface is stationary. The gap between the surfaces, $h(x, y)$, is some arbitrary function of x and y while its dimension is orders of magnitude smaller than either the length (L) or breadth (B) of the bearing pad. The flow within the bearing gap is strictly governed by the 3-dimensional form of momentum and continuity equations. However, to undertake a finite-difference analysis of the full 3-dimensional forms of the equations would be prohibitively expensive and, fortunately, unecessarily elaborate because the extent of the flow in the z-direction is so small compared with the x and y dimensions, pressure variations between the upper and lower surfaces are negligible. It is therefore customary to integrate the x and y momentum equations across the gap thereby eliminating the velocity w directed normal to the bearing surface. The motion of a laminar flow within the bearing is therefore governed by the following system of integro-differential equations.

x-momentum

$$\int_0^h \rho \left(u \frac{\partial u}{\partial x} + v \frac{\partial u}{\partial y}\right) dz = -h \frac{\partial p}{\partial x} + (\tau_{h,xz} - \tau_{0,xz}) \tag{1}$$

y-momentum

$$\int_0^h \rho \left(u \frac{\partial v}{\partial x} + v \frac{\partial v}{\partial y}\right) dz = -h \frac{\partial p}{\partial y} + (\tau_{h,yz} - \tau_{0,yz}) \tag{2}$$

continuity

$$\int_0^h \left(\frac{\partial \rho u}{\partial x} + \frac{\partial \rho v}{\partial y}\right) dz = 0 \tag{3}$$

Equation (3) may alternatively be expressed

$$\frac{\partial (\rho u)_m h}{\partial x} + \frac{\partial (\rho v)_m h}{\partial y} = 0 \tag{4}$$

where

$$(\rho u)_m = \frac{1}{h} \int_0^h \rho u \, dz$$

likewise for $(\rho v)_m$.

To proceed further assumptions must be made about the distributions of velocity within the film. Here we assume that the *shape* of the mean velocity distribution in the film is unaffected by inertia which follows the practice of Osterle and Saibel [11], Constantinescu [12], Burton [13], Smalley, et al. [6] and others. In view of the widespread acceptance of this approach it ought perhaps to be said that the above is not a necessary assumption. We could, for example, let the shape of the profiles depend on some additional parameters whose variation through the flow would be found by taking moments of equations (1) and (2). Approaches of this kind were commonly made in the integral analyses of turbulent boundary layers published in the early 1960's (see Kline, et al. [14] for a collection of such methods). Our current view is that such a practice would be an unnecessary—and hence undesirable—complication of the solution scheme.

For the case of negligible inertial influence, the velocity distribution within the film takes on the well-known parabolic form. Insertion of these profiles into the convective transport terms on the left of equations (1) and (2) enables the integrals in these terms to be found. It is readily deduced that

$$\int_0^h \left(\rho u \frac{\partial u}{\partial x} + \rho v \frac{\partial u}{\partial y}\right) dz = \frac{\partial}{\partial x} (\rho h (\alpha u_m{}^2 - \beta U u_m + \gamma U^2)) + \frac{\partial}{\partial y} (\alpha \rho h u_m v_m) \tag{5}$$

$$\int_0^h \left(\rho u \frac{\partial v}{\partial x} + \rho v \frac{\partial v}{\partial y}\right) dz = \frac{\partial}{\partial x} (\rho h (\alpha u_m v_m - \beta U v_m)) + \frac{\partial}{\partial y} (\alpha \rho h v_m{}^2) \tag{6}$$

Nomenclature

A = convection coefficient in finite-difference equations
B = width of bearing pad
D = pressure-gradient coefficient in finite-difference equations
h = film thickness
h_1 = minimum film thickness at leading edge of bearing pad
h_2 = minimum film thickness at trailing edge of bearing pad
h_3 = maximum film thickness at trailing edge of bearing pad ($=h_2$ if $h = h(x)$ only)
L = length of bearing pad
$\dot{m}_p$ = mass source in finite-difference equations
p = static pressure
$\overline{p}$ = dimensionless static pressure, $\equiv p h_2{}^2/\mu U L$
$\overline{p}_b$ = dimensionless mean pressure over bearing pad, $\equiv \frac{1}{BL} \int_0^B \int_0^L \overline{p} dx dy$
Q = flow rate
$\overline{Q}_i$ = dimensionless flow rate through pad inlet, $\equiv Q_i/U h_1 B$
$\overline{Q}_s$ = dimensionless flow rate through both side edges, $\equiv Q_s/U h_1 B$
Re* = film Reynolds number $\equiv$
$$\frac{U}{\nu L} \frac{(h_2 + h_3)^2}{4}$$
S, S_U, S_p = source terms in finite-difference equations
u = axial velocity
u_m = axial mass-mean velocity, $\equiv$
$$\frac{1}{\rho_m h} \int_0^h u dz$$
v = lateral velocity
v_m = lateral mass-mean velocity, $\equiv$
$$\frac{1}{\rho_m h} \int_0^h v dz$$
x = axial coordinate
y = lateral coordinate
z = cross film coordinate
α, β, γ = coefficients in integral momentum equations
$\delta x, \delta y$ = linear dimensions of control volumes
μ = dynamic viscosity
ν = kinematic viscosity
ρ = density
τ_{xz} = shear stress in x-direction
τ_{yz} = shear stress in y-direction
ϕ = dependent variable

Subscripts
P, E, W, S, N = finite-difference nodes
e, w, s, n = control volume faces
0 = lower (sliding) surface of bearing pad
h = upper (stationary) surface of bearing pad

Superscripts
u = u-velocity
v = v-velocity
* = preliminary value
′ = perturbation

Downloaded 16 Aug 2012 to 165.91.101.108. Redistribution subject to ASME license or copyright; see http://www.asme.org/terms/Terms_Use.cfm

where coefficients α, β, and γ take the constant values

$$\alpha = 1.200; \quad \beta = 0.100; \quad \gamma = 0.133.$$

Equations (5) and (6) are applicable to turbulent flows as well as laminar ones except that the coefficients α, β, and γ take on different values; further details are given in [10].

The assumption of invariance of profile shape to inertial influence also allows the surface-shear stresses to be expressed in terms of the velocity field:

$$\tau_{h,xz} - \tau_{0,xz} = 12\frac{\mu}{h}(\tfrac{1}{2}U - u_m)$$

$$\tau_{h,yz} - \tau_{0,xz} = -12\frac{\mu}{h}v_m \tag{7}$$

Equations (1) and (2) may therefore be expressed in the form

$$\frac{\partial}{\partial x}(\rho h(\alpha u_m{}^2 - \beta U u_m + \gamma U^2)) + \frac{\partial}{\partial y}(\alpha\rho h u_m v_m) = -h\frac{\partial p}{\partial x} + 12\frac{\mu}{h}(\tfrac{1}{2}U - u_m) \tag{8}$$

$$\frac{\partial}{\partial x}(\rho h(\alpha u_m v_m - \beta U v_m)) + \frac{\partial}{\partial y}(\alpha\rho h v_m{}^2) = -h\frac{\partial p}{\partial y} - 12\frac{\mu v_m}{h} \tag{9}$$

Equations (4), (8), and (9) provide a closed set of coupled, nonlinear, partial differential equations in the three dependent variables u_m, v_m, and p. The following section outlines the numerical procedure adopted for solving the discretized forms of these equations. Before considering their solution, however, it should be noted how the above equations differ from those often used previously in bearing film analysis.

Let us note that in the absence of inertia the shear-stress differences in equation (7) could be expressed in terms of the pressure gradients $\partial p/\partial x$ and $\partial p/\partial y$. Such a substitution is not appropriate in our scheme, however, for then equations (8) and (9) could not be used directly. Instead, the task would simplify to the straightforward solution of the Poisson-type Reynolds equation and a *subsequent* (linear) correction of the pressure gradients to account for inertial effects. The magnitude of this correction would be represented by the left hand side of equations (8) and (9) if recast in terms of the non-inertial pressure gradients $\partial p/\partial x$ and $\partial p/\partial y$. This practice has been adopted, for example, by Khalert [1] Milne [15, 16] for infinitely wide bearing pads.

The penalty paid for the forgoing simplification is clearly that the inertial effects on the pressure field cannot be properly accounted for due to the decoupling of the frictional and inertial terms.

3 The Numerical Solution Procedure

3.1 General Principles. The aim of the procedure is to solve equations (4), (8), and (9) yielding velocity fields $u_m(x, y)$ and $v_m(x, y)$ and pressure field $p(x, y)$ which satisfies the momentum and continuity principles over the solution domain. The coupling and nonlinearity of the equations rule out an analytic approach to solution; a finite-difference scheme has therefore been adopted. The method developed has been based on those devised by our colleagues [7, 8]. The adaption of these procedures to solve the *integrated* forms of the momentum and continuity equations that arise in the analysis of bearing flows has, however, necessitated a number of departures from the original schemes. For this reason a complete presentation of the numerical discretization is provided in section 3.2 while section 3.3 summarises the method for solving the resultant set of algebraic equations. As a preliminary, the following paragraphs set out the main elements of the strategy employed.

First, Fig. 2 shows a small section of the Cartesian grid employed; for simplicity a uniform mesh is shown though the procedure itself is formulated to allow an arbitrary spacing of nodes in the x and y directions. It is seen that the nodes for the three dependent variables are situated at different physical locations in space. This practice which follows that of [7], is particularly convenient in enabling an equation for the pressure field to be obtained from the continuity equation. The film height is stored at the points marked with a cross. The discretized forms of the momentum and continuity equations are obtained by apportioning to each node, a small volume of the flow surrounding it; the boundaries of the control volumes are the planes which bisect and are normal to the lines connecting each node with its four neighbours. The set of difference equations linking values at P with those of neighbouring nodes is obtained by integrating the differential equations over the control volume (or, which amounts to the same thing, by applying directly to the control volume the physical principle embodied in the differential equation). Application of this approach enables the x and y momentum equations to be expressed in the linearised form:

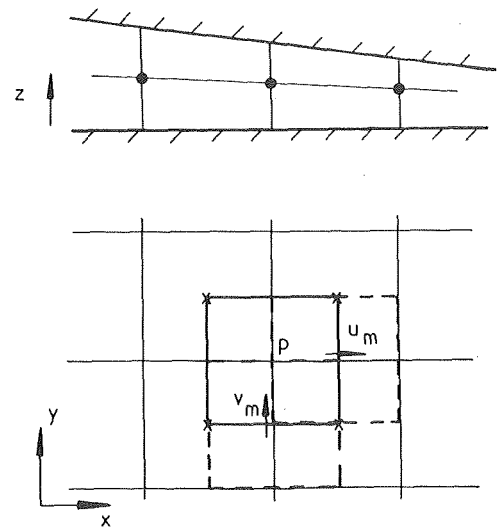

Fig. 2 Finite-difference mesh

$$A_P{}^u u_P = A_W{}^u u_W + A_S{}^u u_S + A_N{}^u u_N + S^u + D^u(p_P - p_E) \tag{10}$$

$$A_P{}^v v_P = A_W{}^v v_W + A_S{}^v v_S + A_N{}^v v_N + S^v + D^v(p_S - p_P) \tag{11}$$

In these equations the A's contain mass fluxes across the control volume boundaries, the D's contain areas on which the relevant pressure differences are acting, and the S's contain frictional terms and the residual parts of the inertial terms that are not accounted for in the (Au)'s and (Av)'s. Note that to avoid double subscripts we have now discarded the m from u_m and v_m; the subscripts P, W, S, and N denote velocity values at the P-nodes and at the "west," "south," and "north" neighbors.

An important feature of (10) and (11) is the absence of the "downstream" velocities u_E and v_E. This occurrence is due partly to the fact that the u (mass-mean) velocities are positive at all nodes (i.e. the flow is everwhere directed from left to right) and partly to the way mass fluxes are evaluated. This feature of the equations enables the velocity field to be found from a noniterative "marching" procedure when the entire pressure field is known and the inlet velocities at the west boundary of the solution domain are given. Of course, the pressure field and inlet velocity profile are unknown initially and must be guessed. The solution of (10) and (11) will consequently give velocities which comply with the momentum equations but not with continuity. The mass-conservation equation must therefore be adapted so that it provides a scheme for correcting the pressure field; details are given in the following section.

3.2 The Finite-Difference Equations. (*a*) *The Momentum Equations.* Fig. 3 shows a representative control volume from which the finite-difference form of the x-momentum equation will be obtained. In integrating the x-momentum equation over the control volume the following assumptions are made.

(i) the mass flow rates across the control-volume faces n, s, and w may be evaluated using velocities which are stored half a cell up-

Downloaded 16 Aug 2012 to 165.91.101.108. Redistribution subject to ASME license or copyright; see http://www.asme.org/terms/Terms_Use.cfm

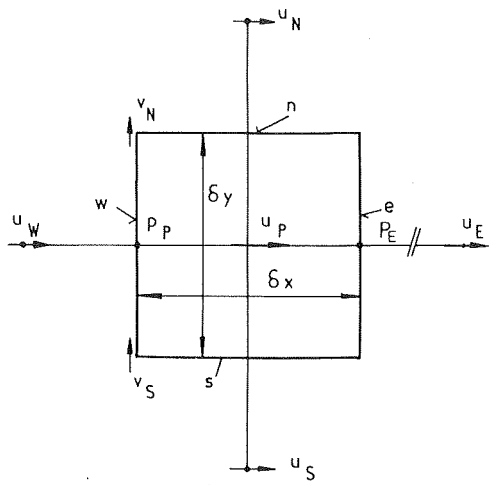

Fig. 3 *x*-momentum control volume

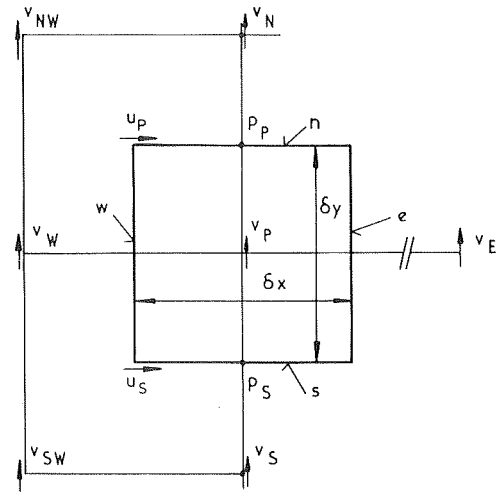

Fig. 4 *y*-momentum control volume

stream (i.e. to the left) and treated as uniform over the respective areas.

(ii) the mass flow rate across face e is obtained from the mass flow rates through the other faces assuming that continuity is satisfied.

(iii) the pressures are uniform over the control volume surfaces.

Further discussion of these assumptions is provided by Patankar [7] and Patankar and Spalding [8]. On observing these principles, integration of equation (8) over the control volume leads to:

$$A_E u_e - A_W u_w + A_N u_n - A_S u_s = D^u(p_P - p_E) + S_U{}^u + S_P{}^u u_P \tag{12}$$

where

$$A_W \equiv (\alpha\rho h)_w u_W \delta y$$

$$A_N \equiv (\alpha\rho h)_n v_N \delta x$$

$$A_S \equiv (\alpha\rho h)_s v_P \delta x$$

$$A_E \equiv A_W + A_S - A_N$$

$$D^u \equiv h_P \delta y$$

$$S_U{}^u \equiv \frac{6\mu}{h_P} U\delta x\delta y + \beta U((\rho h)_s v_P - (\rho h)_n v_N)\delta y - \gamma U^2((\rho h)_e - (\rho h)_w)\delta y$$

$$S_P{}^u \equiv -12\mu\delta x\delta y/h_P$$

In the above the subscripts s, n, w, and e denote that the quantities in question are to be evaluated at the mid points of the corresponding faces using linear interpolation; h_P is the average film height over the cell, again obtained by linear interpolation of the surrounding stored heights.

The question now arises as to how the specific x-momentum at the cell boundaries (u_e, u_w, u_n, u_s) should be chosen. Gosman, et al. [5] were among the first to discover that at high Reynolds numbers stability was improved by choosing the velocities to be those at the node on the upstream side of the cell boundary (rather than as the arithmetic mean of the velocities on either side of the boundary). The adoption of this so-called "upwind-difference" or "donor-cell" scheme in the late 1960's provided a major breakthrough in the numerical solution of elliptic equations; hitherto finite-difference schemes could secure converged solutions only at rather modest Reynolds numbers. This is the scheme we have adopted also. Thus we take:

$$u_e = u_P \text{ and } u_w = u_W,$$

since the flow is always from left to right, and

$$u_s = u_S \text{ or } u_P; \quad u_n = u_P \text{ or } u_N$$

according to whether the flow across the s and n boundaries is from the south or north sides respectively. With this insertion equation (12) can now be expressed as

$$A_P{}^u u_P = A_W{}^u u_W + A_S{}^u u_S + A_N{}^u u_N + D^u(p_P - p_E) + S_U{}^u \tag{13}$$

where

$$A_W{}^u \equiv A_W$$

$$A_S{}^u \equiv \tfrac{1}{2}(A_S + |A_S|)$$

$$A_N{}^u \equiv \tfrac{1}{2}(-A_N + |A_N|)$$

$$A_P{}^u \equiv A_W{}^u + A_S{}^u + A_N{}^u - S_P{}^u$$

The absolute value terms implement the upwind difference scheme. For flow from south to north A_S and A_N are both positive thus $A_N{}^u = 0$ and $A_S{}^u = A_S$. The value of u_p is thus unaffected by u_N.

The finite-difference equation for the lateral velocity v_m is derived along similar lines for the control volume shown in Fig. 4, and is stated below without further comment.

$$A_P{}^v v_P = A_W{}^v v_W + A_S{}^v v_S + A_N{}^v v_N + D^v(p_S - p_P) + S_U{}^v \tag{14}$$

where now

$$A_W{}^v \equiv A_W$$

$$A_S{}^v \equiv \tfrac{1}{2}(A_S + |A_S|)$$

$$A_N{}^v \equiv \tfrac{1}{2}(-A_N + |A_N|)$$

$$A_P{}^v \equiv A_W{}^v + A_S{}^v + A_N{}^v - S_P{}^v$$

and

$$A_W \equiv \tfrac{1}{2}\alpha(\rho h)_w(u_W + u_{SW})\delta y$$

$$A_S \equiv \tfrac{1}{2}\alpha(\rho h)_s(v_W + v_{SW})\delta x$$

$$A_N \equiv \tfrac{1}{2}\alpha(\rho h)_n(v_W + v_{NW})\delta x$$

$$D^v \equiv h_P \delta x$$

$$S_U{}^v \equiv -\beta U(\rho h)_w v_W \delta y$$

$$S_P{}^v \equiv -\frac{12\mu}{h_P}\delta x\delta y + \beta U(\rho h)_e \delta y$$

Equations (13) and (14) represents a set of linearized equations linking the u and v velocities at P with their neighbours to the north, south, and west but *not* to the east.

The absence of this easterly connection means that a noniterative procedure can be used to obtain the u's and v's when the pressure field is known. Suppose, for example, that the velocity field is known along

Downloaded 16 Aug 2012 to 165.91.101.108. Redistribution subject to ASME license or copyright; see http://www.asme.org/terms/Terms_Use.cfm

some rows of nodes—which we shall imagine to be the west line. Then each equation (14) for the row of nodes to the right now relates v_P to its north and south neighbours v_N and v_S; all other terms in the equation are known. The resultant coefficient matrix is thus tridiagonal and the value of the v's is readily obtained by application of the so-called Thomas algorithm (for details see [7] or [8]). With the v's found the convection coefficient in equation (13) may be evaluated and, in a precisely parallel manner, the next row of u's is obtained. The same sequence of operations is now applied to the next row on the right and in this way the whole field is scanned starting at the left boundary where boundary conditions are provided and marching row-by-row to the downstream edge of the pad.

(*b*) *The Pressure-Correction Equation.* The discussion of preceding paragraphs has outlined how the velocity field may be found by a single sweep, row-by-row, across the solution domain; a requirement however was that the pressure distribution should be known. Of course $p(x, y)$ is not known at the start of computation (if it were we should not be concerned with the velocity field); here we outline how, by successive application of the continuity relation to the control volumes surrounding each pressure node we can secure a pressure field in harmony with the velocity field.

Let us suppose that a preliminary estimate has been made of the pressure distribution (perhaps obtained by neglecting entirely inertial effects) and that the corresponding velocity field has been found by solving equations (13) and (14). These estimated values are identified by a star superscript. Thus the velocity and pressure field satisfy

$$A_P{}^u u_P{}^* = A_W{}^u u_W{}^* + A_S{}^u u_S{}^* + A_N{}^u u_N{}^* + D^u(p_P{}^* - p_E{}^*) + S_U{}^u \quad (15)$$

$$A_P{}^v v_P{}^* = A_W{}^v v_W{}^* + A_S{}^v v_S{}^* + A_N{}^v v_N{}^* + D^v(p_S{}^* - p_P{}^*) + S_U{}^v \quad (16)$$

These preliminary values of velocity will not in general satisfy the continuity equation. Thus, if we consider the control volume centred on the pressure node p_P we should find that the mass flow rates into the cell did not sum to zero. That is there will be a mass source $\dot{m}_P$ given by:

$$\dot{m}_P = ((\rho u^* h)_W - (\rho u^* h)_P)\delta y + ((\rho v^* h)_P - (\rho v^* h)_N)\delta x \quad (17)$$

Let us imagine that a correction is now applied to the velocity field, u_p', u_W' etc., (including a corresponding perturbation in the pressure field p_p', p_W' etc.) and that this is such that the momentum and continuity equations are satisfied.

Evidently, from equation (17) the perturbation velocity field will satisfy

$$((\rho u' h)_W - (\rho u' h)_P)\delta y + ((\rho v' h)_P - (\rho v' h)_N)\delta x = -\dot{m}_P \quad (18)$$

Thus, if we neglect the effect of the perturbations on the coefficients of equation (13) there follows

$$A_P{}^u u_P' = A_W{}^u u_W' + A_S{}^u u_S' + A_N{}^u u_N' + D^u(p_P' - p_E') \quad (19)$$

Equations (18) and (19) and the corresponding perturbation equation for v_P' provide a set of equations which if applied simultaneously over the whole field would yield values of p_P', u_P', and v_P' for each cell. However, even if we were to obtain such a simultaneous "solution" further iterations would be necessary because the convection coefficients will in fact be altered by the modifications to the velocity. Because of this inherent nonlinearity, the above equation set is an unnecessarily complicated one. Since iteration will in any case be necessary, all that we need require is that the linking between the p''s and u''s be such that, as we make successive refinements to the perturbation velocity and pressure fields, the magnitude of these perturbations should all approach zero. We shall therefore adopt the much simplified form of equations (19) in which the velocity perturbation u_p' is proportional to the difference in the pressure perturbation on the left and right sides of the cell, i.e.:

$$u_P' = \frac{D^u}{A_P{}^u}(p_P' - p_E') \quad (20)$$

Similarly we write:

$$v_P' = \frac{D^v}{A_P{}^v}(p_S' - p_P') \quad (21)$$

Finally, by inserting equations (20) and (21) and the corresponding equations for u_W' and v_W' above into the continuity equation for the perturbation velocity (18), we may relate the pressure perturbation to be applied at point P to the perturbation at neighbouring nodes:

$$A_P{}^p p_P' = A_W{}^p p_W' + A_E{}^p p_E' + A_N{}^p p_N' + A_S{}^p p_S' - \dot{m}_P \quad (22)$$

where the "A" coefficients involve cell-face areas, densities and the convection coefficients appearing the momentum equations.

Equation (22) expresses the fact that a perturbation in pressure at one point is felt on all sides. So strictly we need to store values of the pressure corrections at all nodes in the solution domain (i.e. a 2-dimensional storage is needed). However, the equation is already much simplified and, in practice it turns out that we can discard, without significant penalty, the east-west connection indicated in (22) and thus hold at any instant the value of the p''s along just a single row. The form of the pressure correction equation actually solved is thus:

$$A_P{}^p p_P' = A_S{}^p p_S' + A_N{}^p p_N' - \dot{m}_P \quad (23)$$

The use of this greatly simplified pressure correction equation is permissible because we demand only that the p'$'$s become negligible as the mass imbalances become vanishingly small. Our aim has been to keep storage demands to an absolute minimum; if storage posed no limitation, slightly faster convergence could possibly be obtained by storing pressure corrections over the whole field. As the pressure corrections (i.e. the p''s) are calculated these are added to the guessed pressure field (the p^*'s); the process of recalculating the velocity field and estimating pressure corrections is successively repeated until the mass source has become negligible. The following section outlines briefly how this is done.

(*c*) *Solution of the Equation Set.* Let us note first that equations (13), (14), and (23) for the velocities and the pressure correction respectively possess the common form

$$A_P{}^\phi \phi_P = A_W{}^\phi \phi_W + A_S{}^\phi \phi_S + A_N{}^\phi \phi_N + S^\phi \quad (24)$$

Since the coefficients A^ϕ are evaluated from upstream conditions, it follows that all variables ϕ can be stored in one-dimensional arrays. The only two-dimensional array required is that for the pressure. (The pressure of course is not one of the variables denoted by ϕ. Its two-dimensional storage is needed to evaluate the source term S_U in the axial momentum equation). The above facts render the solution procedure very economical of computer time and storage. This applies a simple recurrence formula to yield the ϕ-values along the grid line in question taking advantage of the tridiagonal form of the coefficient matrix. The method is noniterative and rapid.

The steps in the present solution procedure may be summarized as follows:

(i) An initial guess is made of the pressure field p^* and the inlet velocities $u_{in}{}^*$; the $v_{in}{}^*$'s are set to zero.

(ii) The coefficients of the axial momentum equation for the first internal u-velocity column are calculated and the equation solved by the tri-diagonal matrix algorithm (TDMA).

(iii) The treatment under (ii) is repeated for the adjacent v-velocity column and the next (i.e. downstream) u-velocity column.

(iv) The coefficients of the pressure correction equation are calculated, the mass sources are evaluated and the equation solved by the TDMA.

(v) The pressures along the column in question are corrected by adding the pressure corrections p' to the corresponding pressures p^*.

(vi) The u-velocities lying downstream of the pressure column and the v-velocities lying along that column are corrected by adding the corrections u' and v' (evaluated from equations (20) and (21) to the corresponding velocities u^* and v^*.

(vii) Steps (iii) to (vi) are repeated successively for all subsequent

Downloaded 16 Aug 2012 to 165.91.101.108. Redistribution subject to ASME license or copyright; see http://www.asme.org/terms/Terms_Use.cfm

columns until the right hand boundary is reached.

(viii) The inlet velocities u_{in} are corrected (see discussion on boundary conditions below).

(ix) Steps (ii) to (viii) are repeated until the mass sources have fallen below some pre-set value (typically 0.1 percent of the inlet mass flow) signifying a converged solution.

3.3 The Grid and Boundary Conditions. The finite-difference grid used for nearly all runs was a uniform, rectangular 11 × 12 mesh with the dependent variables located in a staggered arrangement as discussed in section 3.1. A few validation tests were made with a 16 × 17 grid; in no case did the predicted flow quantities differ by more than 1 percent from those obtained with the coarser grid and for this reason the 11 × 12 mesh was adopted for the bulk of the computations. In the case of the infinite width bearing, which was studied briefly to test the numerical accuracy achieved, an 11 × 3 mesh was employed.[1]

Different boundary condition treatments were needed for pressure and velocities. These are summarized below.

(*a*) Pressure. The pressure has been assumed ambient around the entire domain of solution.

This assumption is a good one for the trailing and side edges of the bearing but less so at the leading edge. A number of workers among them Burton, et al. [17] and Galetuse [18] have shown that inertia effects immediately upstream of the leading edge can result in a "ram pressure" at that location. It would be easy to incorporate this ram pressure into the present computation scheme. We have not done so however, because of the lack of firm evidence about its magnitude.

(*b*) Velocities. The boundary conditions for the velocity are not as easily treated as those for the pressure. The problem is one of interfacing the bearing-film flow with the external flow at the leading and side edges. Here reference has to be made to the expected flow pattern and all edges must be treated individually.

Fig. 5 shows part of the finite-difference grid near the leading edge.

While the lateral inlet velocity v_{in} can adequately be assumed zero, the problem arises as to how to evaluate the inlet velocity u_W. If effects of inertia are negligible, this velocity is simply evaluated with reference to the pressures p_p and p_W. In general, however, the first velocity u_W, is affected by an unknown convective transport of momentum from upstream regions lying outside the domain of solution. A remedy is suggested below.

At inlet a guess is made for u_{in}. The velocity u_W is then evaluated from a slightly modified version of equation (13) for the half control volume as shown in Fig. 5. After the velocities u_P and v_P and an improved pressure p_P have been determined, the first velocity u_W is corrected according to equation (20) applied to W rather than P and with $p_W' = 0$. An improved inlet velocity is then evaluated by applying the continuity eqation to this semicontrol volume. This scheme proved to be satisfactory for all flow conditions investigated.

[1] Three nodes in the y direction is the minimum that can be used in our scheme to prescribe zero variations in that direction.

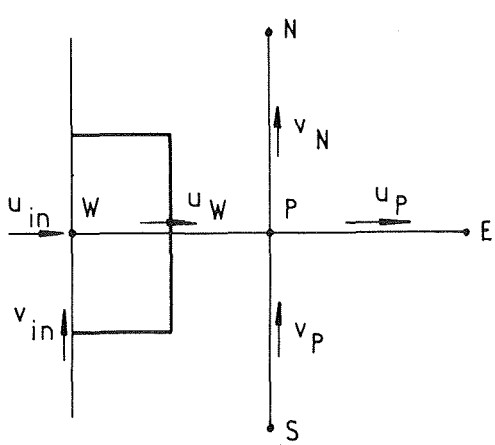

Fig. 5 Inlet boundary

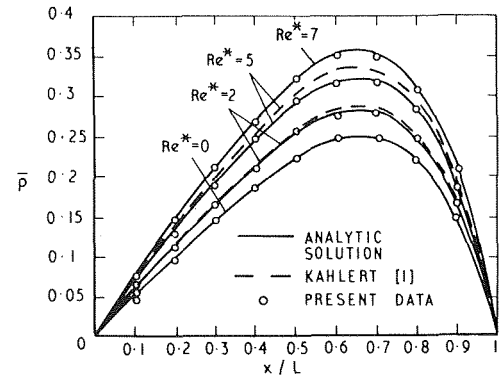

Fig. 6(*a*)

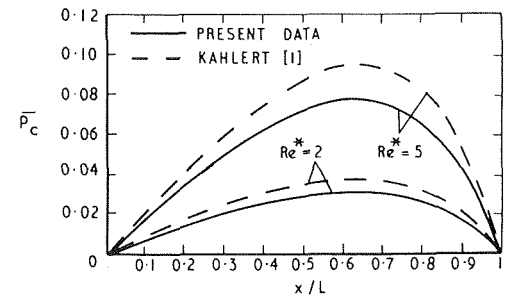

Fig. 6(*b*)

Fig. 6 Pressure distributions in infinite-width pad, $h_1/h_2 = 2$

For the side edges, no boundary values for the v-velocities are needed. This is because fluid always flows outwards, and there will be no lateral momentum transport into the solution domain from outside regions. Boundary values for the axial velocities u are, however, required. It has been assumed here that the gradient du/dy near the side edges is zero. Although this assumption is not entirely realistic it was found that the values of the boundary velocities had a negligible effect on the resulting pressure and velocity fields.

4 Application For Flows in Plane Pads

The first example relates to the infinitely wide plane pad. Here lateral velocities are absent and one may solve analytically the 2nd-order equation governing the pressure variation within the pad; the resultant formulae for the flow rate and the pressure variation do not seem to have been quoted before and for this reason are given in the Appendix.

For the pressure distribution Figs. 6 (*a*) and (*b*) compares our numerical results, obtained with a 11 × 3 uniform grid, with the exact analytical solution and with the results of Kahlert [1] (the latter are identical to the first order inertial correction of Milne [16]). The ratio of inlet to exit film heights is 2:1. Kahlert's procedure, it will be realized took only a linearized account of the inertial terms. It is clear that as the level of Re* is progressively raised the linearized procedure progressively overpredicts the effects of inertia on the pressure distribution, the error in peak pressure being 5 percent for Re* = 5 (or 20 percent for the inertial pressure correction). From Fig. 7 the flow rate is seen to drop as the Reynolds number is raised; again the numerical solution with 11 equispaced nodes in the x-direction achieves almost complete agreement with the analytical solution.

Now let us examine some features of finite-width bearings. Fig. 8 shows pressure distributions for a square thrust pad ($B/L = 1$) with a contraction ratio of 2:1. Numerical solutions are shown for Re* up to 6. Evidently, the inertial effects have a negligible influence on the shape of the pressure profiles but the general level of the mean pressure $\bar{p}_b$ increases with Re*; indeed, the relative sensitivity of $\bar{p}_b$ to inertial effects is very similar to that for an infinite-width bearing as can be seen on comparing Figs. 7 and 9. We may therefore conclude

Downloaded 16 Aug 2012 to 165.91.101.108. Redistribution subject to ASME license or copyright; see http://www.asme.org/terms/Terms_Use.cfm

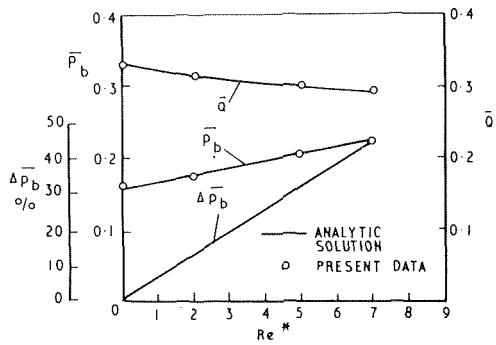

Fig. 7 Mean pressure and flow rate in infinite width pad, $h_1/h_2 = 2$

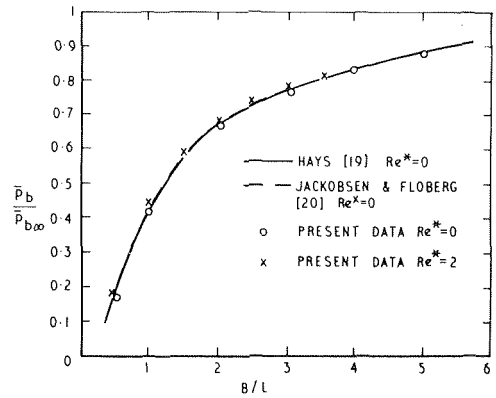

Fig. 10 Normalized mean pressures, in pads of varying width-to-length ratio, $h_1/h_2 = 2$, Re* = 0 and Re* = 2

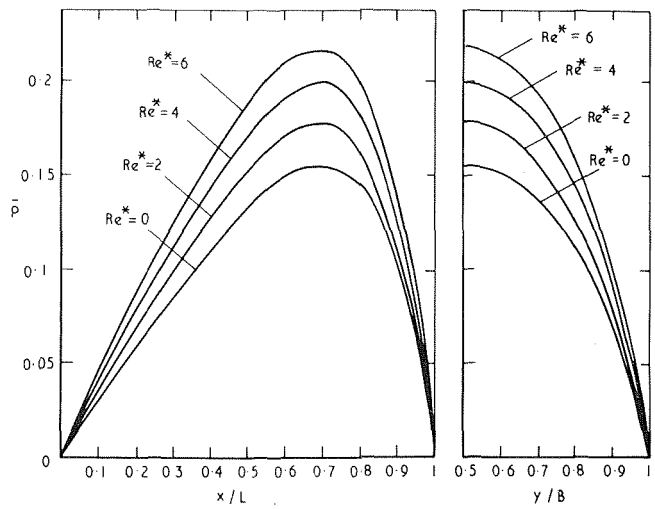

Fig. 8 Pressure profiles in square pad, $h_1/h_2 = 2$

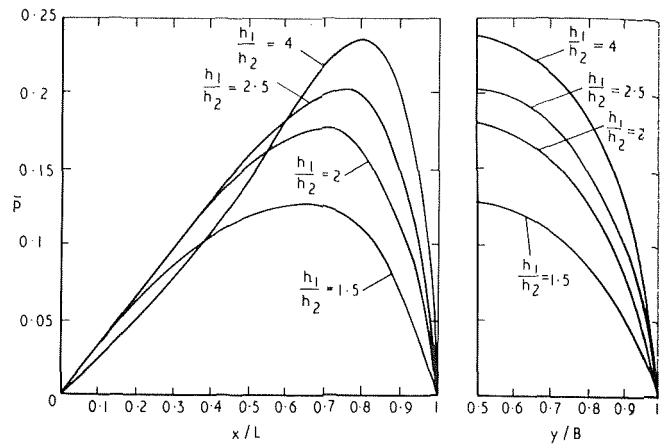

Fig. 11(*a*) Pressure profiles in square pad, Re* = 2

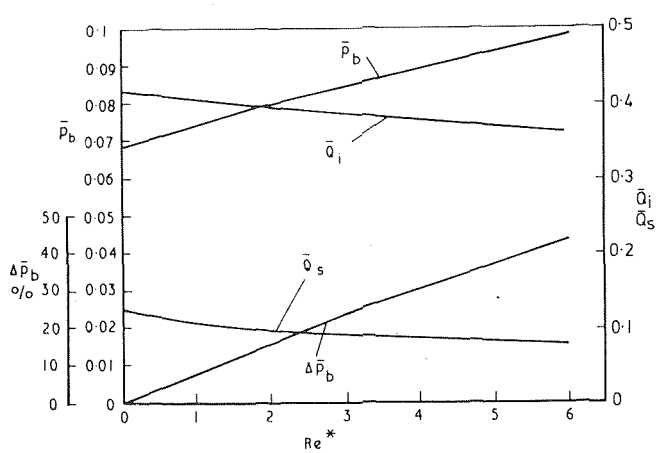

Fig. 9 Mean pressure and flow rate in square pad, $h_1/h_2 = 2$

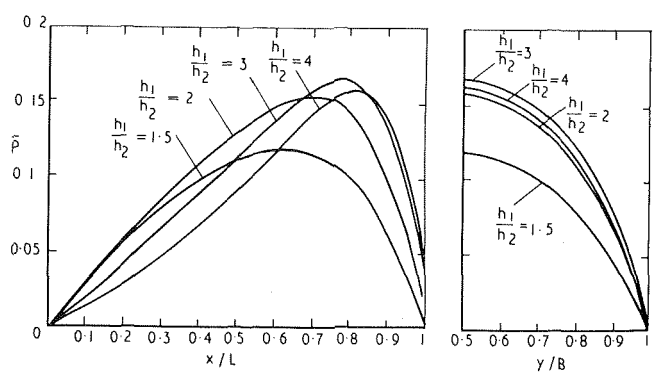

Fig. 11(*b*) Pressure profiles in square pad, Re* = 0

that the mean pressure, if normalized by that for the infinite-width bearing, should be almost independent of the Reynolds number Re*. Fig. 10 confirms this conclusion. It shows the normalised mean pressure for Re* = 0 and Re* = 2 for width-to-length ratios ranging from 0.5 to 5. The numerical solutions are compared with results of Hays [19] and Jakobsen and Floberg [20]. Agreement is seen to be virtually complete for Re* = 0. Fig. 9 shows how the flow rates through the square pad vary with Reynolds number. Both the inlet and the leakage flow rates diminish with Reynolds numbers. For this particular geometry they decrease by similar absolute amounts; consequently the lubricant flux out of the trailing end of the pad is virtually the same throughout.

Although the effect of inertia on the pressure profiles is virtually indepedent of B/L it is substantially dependent on the change in film height from inlet to exit. These features are well brought out in Figs. 11 (*a*) and 11 (*b*) which show mid-plane pressure profiles in the square pad for contraction ratios ranging from 1.5 to 4. Fig. 11 (*a*) gives results for Re* = 2 while Fig. 11 (b) relates to the noninertial case. In both cases, as the contraction ratio is increased, the pressure profile becomes more asymmetric with the peak pressure occurring at larger values of x/L. While, for Re* = 0, the peak pressure reaches a maximum for $h_1/h_2 = 3.5$, it appears to rise indefinitely with h_1/h_2 at a

Downloaded 16 Aug 2012 to 165.91.101.108. Redistribution subject to ASME license or copyright; see http://www.asme.org/terms/Terms_Use.cfm

reduced Reynolds number of 2. As a result, it is seen from Fig. 12 that the mean bearing pressure continues to increase marginally for values of h_1/h_2 up to 7 while, if inertia is neglected, there is a sharp diminuition for contraction ratios greater than 2.3. Thus, at a contraction ratio of 4:1 the mean bearing pressure at Re* = 2 is 63 percent higher then indicated by the noninertial solution. An extensive survey of the calculated effect of geometric and flow parameters is given by Leschziner [21]. Here therefore, we shall, as a final example, consider just the case where the pad height varies with both x and y; that is, the pad is tilted as indicated in Fig. 13 with $h_1/h_2 = 2.5$ and $h_3/h_2 = 1.5$.

Fig. 12 shows several isobars within the pad (normalized by the maximum pressure); the results are specifically for Re* = 0 but there is an insignificant effect of Reynolds number on the shape of these contours. As would be expected, the position of maximum pressure is displaced towards the corner of minimum film height. The effect of the inertial terms on the level of pressure in the pad emerges from Fig. 14, which shows pressure profiles along constant-x and constant-y lines passing through the point of maximum pressure.

Because of the geometric differences between the symmetric and asymmetric pads considered, we shall not attempt a quantitative comparison of the effect of inertia on the pressure levels. However, a qualitative comparison quickly reveals inertial effects to be very similar in both cases.

Finally, the effect of inertia on the flow rate in the asymmetric pad is illustrated by Fig. 15. As in the symmetric case both the inlet and side leakage velocities are progressively retarded as Re* increases. It is interesting to note that the symmetry of the inlet velocity profiles remains almost intact despite the significant tilt in the y-direction. Furthermore, the side leakage velocities at both side edges are almost identical although the lateral velocity profiles are, of course, no longer antisymmetric, with respect to the line $y = B/2$.

Concluding Remarks

The numerical scheme for laminar flow forms a preliminary but important step toward the formulation of a more general procedure for the solution of turbulent inertial flow in bearing films. The main aim has, therefore, been to examine the scheme's performance under extreme conditions. Thus, high contraction ratios and film Reynolds numbers have been prescribed to demonstrate that stability and computational efficiency are not unduly affected. The study, if looked upon as being self contained, allows the general conclusion that inertia is not an unimportant aspect in the design of bearings for optimum operation, even then when film thickness gradients are uniform and the film Reynolds number is realistically low.

Inertial effects are, of course, of far greater inportance in stepped and pocketed bearings. Since no restrictions have been imposed on the film-thickness distribution, the present scheme may also be applied profitably to such geometries almost without modifications.

Acknowledgment

The work reported in this paper has been supported by the Science Research Council of Great Britain through grant B/RG/5223/3 as part of a collaborative programme of research with the Institute of Tribology at the University of Leeds/England. Authors names appear alphabetically.

References

1 Kahlert, W., "Der Einfluß der Trägheitskräfte bei der hydrodynamischen Schmiermitteltheorie," *Ing. Arch.*, Vol. 16, 1948, p. 321.

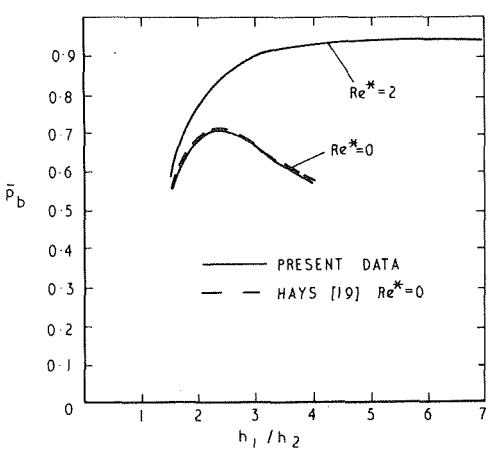

Fig. 12 Mean pressure in square pad, Re* = 0 and Re* = 2

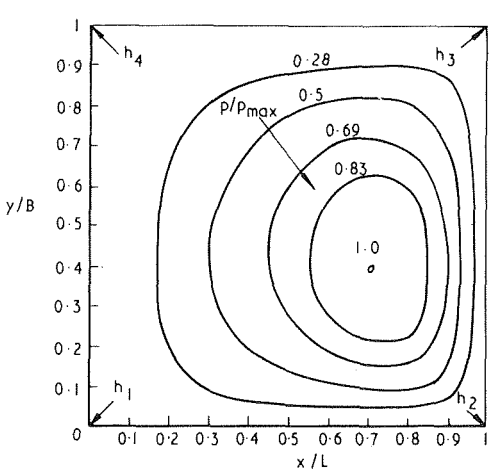

Fig. 13 Isobars in asymmetric square pad, $h_1/h_2 = 2.5$, $h_3/h_2 = 2.5$, Re* = 0

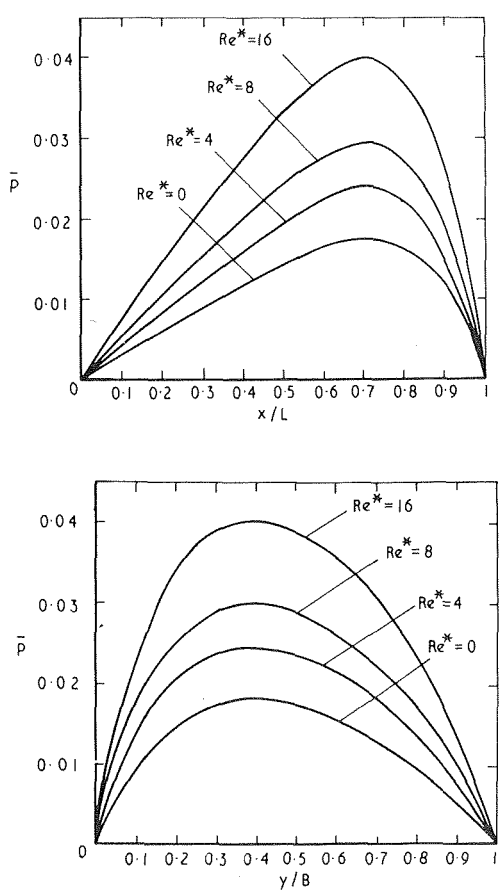

Fig. 14 Pressure profiles in asymmetric square pad, $h_1/h_2 = 2.5$, $h_3/h_2 = 1.5$

Downloaded 16 Aug 2012 to 165.91.101.108. Redistribution subject to ASME license or copyright; see http://www.asme.org/terms/Terms_Use.cfm

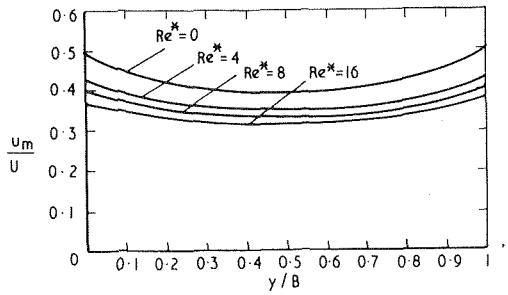

Fig. 15(*a*)

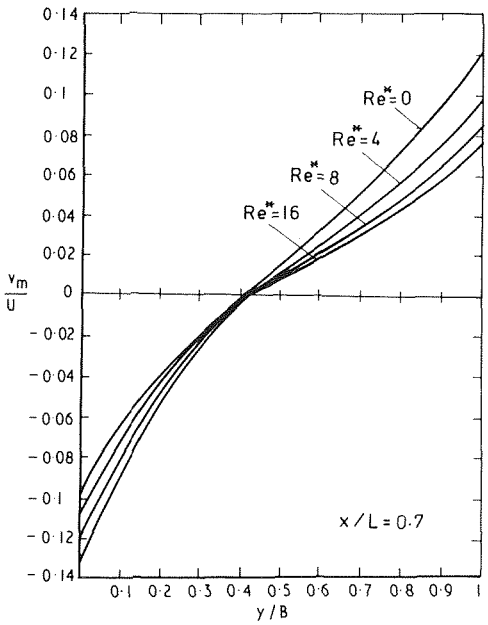

Fig. 15(*b*)

Fig. 15 Inlet and side leakage mass-mean velocity distributions in asymmetric pad, $h_1/h_2 = 2.5$, $h_3/h_2 = 1.5$

2 Brand, R. S., "Inertia Forces in Lubricating Films," TRANS. ASME, Vol. 77, 1955, p. 363.

3 Kamal, M. M., "Separation in the Flow Between Eccentric Rotating Cylinders," *ASME Journal of Basic Engineering*, Vol. 88, 1966, p. 717.

4 Launder, B. E., and Ying, W. M., "Numerical Solution of Flow Between Rotating Cylinders," *Journal of Mechanical Engineering* Science, Vol. 14, 1972, p. 400.

5 Gosman, A. D., Pun, W. M., Runchal, A. K., Spalding, D. B., and Wolfshtein, M., *Heat and Mass Transfer in Recirculating Flows*, Academic Press, London, 1969.

6 Smalley, A. J., Vohr, J. H., Costelli, V., and Wachmann, C., "An Analytical and Experimental Investigation of Turbulent Flow in Bearing Films Involving Convective Fluid Inertia Forces," ASME Paper 73-Lubs-1, 1973.

7 Patankar, S. V.: "Numerical Prediction of Three-Dimensional Flows," *Studies in Convection 1*, Edited by B. E. Launder, Academic Press, London, 1976.

8 Patankar, S. V., and Spalding, D. B., "Numerical Predictions of Three-Dimensional Flows," Imperial College, London, MED Rep. EF/TN/A/46, 1972.

9 Gosman, A. D., and Pun, W. M., "Calculation of Recirculating Flows," Imperial College, London, MED Rep. HTS/74/2, 1973.

10 Launder, B. E., and Leschziner, M., "Flow in Finite-Width Thrust Bearings Including Inertial Effects. 2—Turbulent Flow," ASME JOURNAL OF LUBRICATION TECHNOLOGY, published in this issue pp. 339–345.

11 Osterle, F., and Saibel, E. A., "On the Effect of Lubricant Inertia in Hydrodynamic Lubrication," *ZAMP*, Vol. 6, 1955, p. 334.

12 Constantinescu, V. N., "On the Influence of Inertia Forces in Turbulent and Laminar Self-Acting Films," ASME Journal of Lubrication Technology, Vol. 92, 1970, p. 473.

13 Burton, R. A., "Approximation in turbulent film analysis," ASME Paper No. 73-Lubs-17, 1973.

14 Kline, S. J., Morkovin, M. V., and Cotterell, D., Proc AFOSR—Stanford Conference on the Calculation of Turbulent Boundary Layers, Stanford University, 1968.

15 Milne, A. A., "On the Effect of Lubricant Inertia in the Theory of Hydrodynamic Lubrication," ASME *Journal of Basic Engineering*, Vol 81, 1959, p. 239.

16 Milne, A. A., "Inertia Effects in Self-Acting Bearing Lubrication Theory," Int. Symposium on Lub. Wear, Houston McCutchon Publ. Co., 429, 1963.

17 Burton, R. A., Carper, H. J., and Hsu, Y. C., "An Experimental Study and Analysis of Turbulent film Tilted Pad Bearings," ASME Paper No. 73-Lubs-20, 1973.

18 Galetuse, S., "Experimental Study on the Interference of Inertia and Friction Forces in Turbulent Lubrication," ASME Paper No. 73-Lubs-12, 1973.

19 Hays, D. F.: "Plane sliders of finite width," *Trans. ASLE*, Vol. 1, 1958, p. 233.

20 Jakobsen, B., and Floberg, L., "The Rectangular Plane-Pad Bearing," *Trans. Chalmers Univ. Techn. Gothenburg*, Vol. 203 1958.

21 Leschziner, M., "Turbulent Flow in Finite-Width Bearing Films Including Turbulence Transport and Inertia Effects," PhD thesis, University of London, 1976.

APPENDIX

Analytical Solution For an Infinitely Wide Slider Bearing

On neglecting gradients with respect to y in equation (8) we obtain the form appropriate to an infinitely wide bearing. On rearranging we find:

$$\frac{dp}{dx} = \frac{12\mu}{h^2}\left(\frac{U}{2} - u_m\right) + \frac{\rho}{h}\left(\alpha u_m{}^2 - \gamma U^2\right)\frac{dh}{dx} \tag{A1}$$

together with the continuity equation

$$\frac{d}{dx}(\rho h u_m) = 0 \tag{A2}$$

We consider a plane slider of length L for which the film thickness may be written:

$$h(x) = a - bx \tag{A3}$$

Given the boundary conditions:

$$p(o) = p(L) = 0 \tag{A4}$$

integration of equation (A1) leads to the following solutions for the flow rate Q and the pressure distribution $p(x)$:

$$Q = \frac{6\mu}{T_1} + \sqrt{\left(\frac{6\mu}{T_1}\right)^2 + \frac{T_2}{T_1}} \tag{A5}$$

where

$$T_1 \equiv \alpha\rho b$$

$$T_2 \equiv -\frac{2}{\dfrac{1}{(a-bL)^2} - \dfrac{1}{a^2}} \times \left[\gamma\rho U^2 b \cdot \ln\left(\frac{a-bL}{a}\right) - 6\mu U\left(\frac{1}{a-b_L} - \frac{1}{a}\right)\right]$$

$$p(x) = \frac{6\mu U}{b}\left[\frac{1}{(a-bx)} - \frac{1}{a}\right] - \frac{T_2}{2b}\left[\frac{1}{(a-bx)^2} - \frac{1}{a^2}\right] - \gamma\rho U^2\left[\frac{1}{\ln(a-bx)} - \frac{1}{\ln a}\right] \tag{A6}$$

Downloaded 16 Aug 2012 to 165.91.101.108. Redistribution subject to ASME license or copyright; see http://www.asme.org/terms/Terms_Use.cfm